Floquet stability and Lagrangian statistics of a nonlinear time-dependent ABC dynamo

Calum S. Skene* and Steven M. Tobias
Department of Applied Mathematics, University of Leeds, Leeds LS2 9JT, United Kingdom

(Received 25 January 2023; accepted 28 July 2023; published 28 August 2023)

The Lagrangian statistics of a time-dependent ABC flow are considered, with time dependence introduced via harmonic oscillation with frequency Ω. By calculating the finite-time Lyapunov exponents (FTLEs), the Lagrangian statistics of the system are determined for a range of values of Ω. These statistics are calculated for the kinematic regime where the flow remains an ABC flow, the nonlinear regime with dynamo action present, and a second hydrodynamic state reached through instability of the original ABC flow. It is found that there are significant differences between these three states, with most cases showing a decrease in their FTLEs as the flow deviates from its original ABC form. Furthermore, these changes are highly dependent on Ω, with lower frequencies leading to higher FTLEs in the nonlinear regime, and unstable regimes. By examining the Lagrangian statistics with respect to the dynamo behavior observed, we discuss their potential relevance to nonlinear saturation, self-killing dynamos, and the importance of the initial hydrodynamic state. The numerical code developed for this project is also available.

DOI: 10.1103/PhysRevFluids.8.083701

I. INTRODUCTION

In an electrically conducting fluid, the coupling between the velocity field and magnetic field can lead to a self-sustaining magnetic field. This phenomena is termed dynamo action, and is an important physical process underpinning the behavior of many astrophysical flows [1]. The Lagrangian properties of dynamo flows have been conjectured to play a key role in the kinematic and dynamic properties of dynamo action; certainly, this is the case in the kinematic regime at asymptotically high magnetic Reynolds number (Rm)—the so-called fast dynamo problem. Dynamical systems theory applied to fast dynamo action demonstrates that the topological entropy of the flow bounds the asymptotic growth rate of the dynamo [2]; see also Ref. [3]. This rules out the possibility of fast dynamo action for integrable flows and shows that chaotic particle paths are required for a flow to be a fast dynamo.

These results have led to a sustained interest in the Lagrangian properties of saturated dynamo flows. It is hoped that an analysis of such statistics can lead to some progress on the thorny issue of how dynamos saturate. It is clear that the mechanism for dynamo saturation is not universal—dynamos saturate in different ways. For example, large-scale dynamos, where the field is generated on scales larger than a typical velocity scale, may saturate through a modification of the degree of breaking of reflectional symmetry of the flow (so-called α-quenching see, e.g., Ref. [4]) or by

*Corresponding author: c.s.skene@leeds.ac.uk

modifying the properties of large-scale shear flows. It is fair to say that the first mechanism described above is more contentious than the second, and there are fundamental uncertainties about the level at which large-scale magnetic fields saturate [5] and indeed how long it takes to reach saturation (see, e.g., the detailed discussion in Ref. [6]); these can be linked to the irreversibility in the dynamo system, which is often measured by the degree to which magnetic helicity is conserved [7–9].

It is an interesting question as to what can be determined about the mechanism for dynamo saturation from a consideration of the Lagrangian statistics. Since growth of a magnetic field relies on stretching overcoming the dissipative action of magnetic diffusion, it could be that dynamos saturate (and become statistically marginal) in the nonlinear regime by either reducing the stretching (which would be manifested as a suppression of the chaos in the high Rm limit), enhancing the diffusion, or a combination of the two. How the magnetic field might act so as to reduce the stretching is undetermined. It might be that the field acts so as to reduce the amplitude of dynamo flow back to the marginal state—i.e., the flow amplitude might be reduced so $\mathrm{Rm} \approx \mathrm{Rm}_c$ for dynamo action. This drastic intervention of the flow seems unlikely at high Rm (as argued in Cattaneo and Tobias [10]). More likely is that the field acts to reduce the amplitude of the flow somewhat but also suppresses its stretching properties in a subtle manner [11].

This suppression of chaos was shown to be important in a simplified 2.5-dimensional dynamo—here a 2.5-dimensional flow is one that has all three components of the velocity but each component only depends on two spatial coordinates. To maintain two-dimensionality in the nonlinear regime, the Lorentz force was projected back onto the z-invariant velocity [11]. However, firm conclusions for models that include the full Lorentz force in three dimensions are much more difficult to draw. A variety of investigations have been carried out on the Lagrangian properties of saturated dynamo states for a variety of driving mechanisms; not all of these have included a description of the stretching as measured by the Lyapunov exponents.

Zienicke *et al.* [12] considered a forcing based on the steady ABC flow at moderate scale. This flow, with standard parameters, is known to be weakly chaotic; however, at high Re this flow goes unstable to a flow with a range of spatial scales and complicated time dependence. At moderate Reynolds number (Re) and Rm, they found that the growth of a large-scale field can excite velocity modes that can lead to the mean Lyapunov exponents of the saturated state being much larger than that of the kinematic flow, as the flow has many more excited modes in the nonlinear state.

Rempel *et al.* [13] considered the Lagrangian properties of the velocity field of a helical magnetohydrodynamic (MHD) dynamo, with moderate scale, steady forcing. In addition to computing the Lagrangian coherent structures, they also calculated the statistics of the finite-time Lyapunov exponents (FTLEs) and showed that these decay as a linear function of magnetic energy of the saturated dynamo.

Homann *et al.* [14] considered dynamo action in a forced Taylor-Green system and analyzed the statistical properties of both the velocity and magnetic fields in Eulerian and Lagrangian frameworks. They found that these statistics are changed between the kinematic and saturated regimes, with the saturated trajectories aligning more with the mean magnetic field and the probability density functions (PDFs) of the magnetic field changing to quasi-Gaussian. Moreover they observed a dramatic increase of the correlation time of the velocity and magnetic fields in the saturated regime. However, for this flow, the stretching properties as given by the FTLEs remained unmeasured.

Of particular relevance to our study is that of Brummell *et al.* [15], who considered an ABC flow with an added harmonic time dependence which oscillates the ABC flow along the line $x = y = z$. By introducing this time dependence, the chaotic nature of the original ABC flow is enhanced, with the time-dependent flow showing decreased areas of integrability. The degree of chaos induced in the flow depends on the frequency of the oscillation of the imposed flow (or forcing) (see also Ref. [16]).

This is confirmed by considering the FTLEs of the flow. It is shown that this added chaos aids kinematic dynamo action, with the time-dependent ABC flow showing stronger growth rates, as well as behaving as a quick dynamo, i.e., a dynamo "that reaches a neighborhood of its maximal growth rate quickly as a function of Rm" [17]. Brummell *et al.* [15] also considered the nonlinear regime by

performing simulations of the coupled Navier-Stokes and induction equations, where the ABC flow is initially sustained by a body forcing. Although in all cases the flow is a kinematic dynamo, for some frequencies of the oscillations, the dynamo is not sustained in the nonlinear regime and decays until only a turbulent hydrodynamic stated termed U_1 is left. Note that this secondary hydrodynamic state can also be reached through hydrodynamic instability of the original ABC flow.

Our current paper builds upon the work of Brummell *et al.* [15] through calculating the FTLEs of the flow in both the nonlinear regime where the Lorentz force is saturating the dynamo and also for the flow U_1. This involves solving the coupled Navier-Stokes and induction equations together with tracking Lagrangian particles. By calculating the FTLEs in these two flow regimes, we hope to further elucidate the dynamics responsible for dynamo saturation, as well as to explain why some dynamos are unable to sustain themselves in the nonlinear regime.

As well as calculating the FTLEs, we also consider the Floquet stability [18] of the time-dependent ABC flow to both hydrodynamic and magnetic perturbations. In this manner, all the unstable directions of the original flow together with their growth rates can be systematically captured. The paper proceeds as follows: Section II outlines the mathematical and numerical setup, containing the details of the governing equations, Floquet stability analysis, and FTLEs. The results are then presented in Sec. III, with conclusions subsequently being offered in Sec. IV.

II. MATHEMATICAL AND NUMERICAL SETUP

A. Formulation: Governing equations and numerical methods

The system is governed by the magnetic induction and Navier-Stokes equations, which in nondimensional form are

$$(\partial_t - \mathrm{Rm}^{-1}\nabla^2)\boldsymbol{B} = \boldsymbol{\nabla} \times (\boldsymbol{U} \times \boldsymbol{B}), \tag{1}$$

$$(\partial_t - \mathrm{Re}^{-1}\nabla^2)\boldsymbol{U} + \boldsymbol{U} \cdot \boldsymbol{\nabla}\boldsymbol{U} = -\boldsymbol{\nabla} p + \boldsymbol{J} \times \boldsymbol{B} + \boldsymbol{F}, \tag{2}$$

$$\boldsymbol{\nabla} \cdot \boldsymbol{U} = \boldsymbol{\nabla} \cdot \boldsymbol{B} = 0. \tag{3}$$

The nondimensional variables are the fluid velocity $\boldsymbol{U}$, magnetic field $\boldsymbol{B}$, pressure p, and electric current $\boldsymbol{J} = \boldsymbol{\nabla} \times \boldsymbol{B}$. By nondimensionalizing time with respect to a typical turnover time of the flow (U) and space with respect to the length scale of the domain (L), the nondimensional parameters of Reynolds number $\mathrm{Re} = UL/\nu$ and magnetic Reynolds number $\mathrm{Rm} = UL/\eta$ have been introduced. Moreover, in this nondimensionalization, the field is measured in units of the Alfvén speed. The domain is taken to be $(x, y, z) \in [0, 2\pi]^3$ with periodic boundary conditions. Following Brummell *et al.* [15], the external (Re-dependent) forcing term $\boldsymbol{F}$ is chosen such that in the absence of magnetic field there exists an order unity solution for the velocity field $\boldsymbol{U}_0$ given by

$$\begin{aligned}\boldsymbol{U}_0 = &(\sin(z + \epsilon \sin(\Omega t)) + \cos(y + \epsilon \sin(\Omega t)),\\ &\sin(x + \epsilon \sin(\Omega t)) + \cos(z + \epsilon \sin(\Omega t)),\\ &\sin(y + \epsilon \sin(\Omega t)) + \cos(x + \epsilon \sin(\Omega t))).\end{aligned} \tag{4}$$

For $\epsilon = 0$, this flow corresponds to an ABC flow with $A = B = C = 1$. However, by varying ϵ, the flow is allowed to wobble around the ABC state with amplitude ϵ and angular frequency Ω. The initial kinetic energy density is displayed in Fig. 1, showing that it has large scale structures. For low Re, this flow is hydrodynamically stable.

To solve this system numerically, we first replace the magnetic induction equation for $\boldsymbol{B}$ with an equation for the magnetic vector potential $\boldsymbol{A}$ defined such that $\boldsymbol{B} = \boldsymbol{\nabla} \times \boldsymbol{A}$ and with $\boldsymbol{A}$ taken to satisfy the Coulomb gauge condition $\boldsymbol{\nabla} \cdot \boldsymbol{A} = 0$. The resulting system is solved numerically using spectral methods via the open-source partial differential equation (PDE) solver DEDALUS [19]. A resolution of $96 \times 96 \times 96$ is used for all dynamo calculations when particles are not being tracked

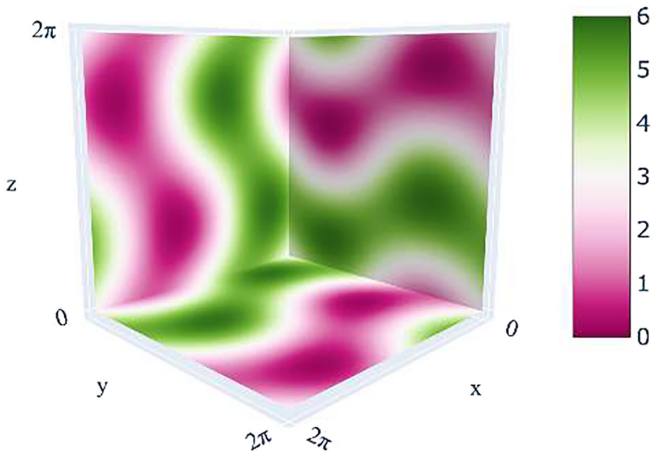

FIG. 1. Contour plot of the initial kinetic energy density connected with $\boldsymbol{U}_0$.

(see the next section) to ensure that the resolution is high enough to prevent spurious dynamo solutions [6]. Two-thirds dealiasing is used to treat all nonlinear terms.

B. Floquet stability analysis

The hydrodynamic state $\boldsymbol{q}_0 = (\boldsymbol{B}, \boldsymbol{U}, p)^T = (\boldsymbol{0}, \boldsymbol{U}_0, P_0)^T$ (with P_0 found through rearrangement of the momentum equation) is an exact periodic solution to Eqs. (1)–(3). Therefore, the stability of the periodic solution $\boldsymbol{q}_0$ to perturbations can be found via a Floquet stability analysis [18] (though traditionally the stability of such flows to dynamo action has usually been found by time stepping). To this end, we first rewrite Eqs. (1)–(3) for the state $\boldsymbol{q} = (\boldsymbol{B}, \boldsymbol{U}, p)^T$ in the more general form

$$\boldsymbol{M}\frac{\partial \boldsymbol{q}}{\partial t} = \boldsymbol{\mathcal{N}}(\boldsymbol{q}, \boldsymbol{F}), \tag{5}$$

where the matrix

$$\boldsymbol{M} = \begin{pmatrix} 1 & 0 & 0 \\ 0 & 1 & 0 \\ 0 & 0 & 0 \\ 0 & 0 & 0 \end{pmatrix} \tag{6}$$

ensures there is no time-derivative term in the continuity equation, or solonoidal condition for $\boldsymbol{B}$, and the operator

$$\boldsymbol{\mathcal{N}} = \begin{pmatrix} \nabla \times (\boldsymbol{U} \times \boldsymbol{B}) + \mathrm{Rm}^{-1}\nabla^2 \boldsymbol{B} \\ -\boldsymbol{U} \cdot \nabla \boldsymbol{U} - \nabla p + \boldsymbol{J} \times \boldsymbol{B} + \mathrm{Re}^{-1}\nabla^2 \boldsymbol{u} + \boldsymbol{F} \\ \nabla \cdot \boldsymbol{U} \\ \nabla \cdot \boldsymbol{B} \end{pmatrix} \tag{7}$$

represents the right-hand side of the equations. We then linearize these equations about $\boldsymbol{q}_0$ to give the linearized equations

$$\boldsymbol{M}\frac{\partial \boldsymbol{q}'}{\partial t} = \boldsymbol{A}(t)\boldsymbol{q}', \tag{8}$$

where

$$\boldsymbol{A}(t) = \left.\frac{\partial \boldsymbol{\mathcal{N}}}{\partial \boldsymbol{q}}\right|_{\boldsymbol{q}=\boldsymbol{q}_0(t)}. \tag{9}$$

As Eq. (8) is linear, the solution at any time t can be obtained from an initial condition at time t_0 using the state-transition matrix $\boldsymbol{\Psi}(t, t_0)$ via $\boldsymbol{q}'(t) = \boldsymbol{\Psi}(t, t_0)\boldsymbol{q}'(t_0)$. The matrix $\boldsymbol{\Psi}(t_0 + T, t_0)$ that propagates a state forward by one period T is known as the monodromy matrix. By taking the eigenvalue decomposition of this matrix, i.e., by solving $\boldsymbol{\Psi}(t_0 + T, t_0)\boldsymbol{q}_i(t_0) = \mu_i \boldsymbol{q}_i(t_0)$, we can write any perturbation in terms of the decomposition as

$$\boldsymbol{q}' = \sum_i \boldsymbol{q}_i \exp(t\lambda_i), \tag{10}$$

where $\lambda_i = \ln(\mu_i)/T$. The stability of the flow can then be determined from the Floquet multipliers μ_i, with the flow stable if $|\mu_i| < 1$ and unstable if $|\mu_i| > 1$.

Our linearized Eqs. (8) can be written as

$$(\partial_t - Re^{-1}\nabla^2)\boldsymbol{U}' + \boldsymbol{U}_0 \cdot \boldsymbol{\nabla}\boldsymbol{U}' + \boldsymbol{U}' \cdot \boldsymbol{\nabla}\boldsymbol{U}_0 = -\boldsymbol{\nabla} p', \tag{11}$$

$$\boldsymbol{\nabla} \cdot \boldsymbol{U}' = 0, \tag{12}$$

$$\left(\partial_t - \mathrm{Rm}^{-1}\nabla^2\right)\boldsymbol{B}' = \boldsymbol{\nabla} \times (\boldsymbol{U}_0 \times \boldsymbol{B}'), \tag{13}$$

$$\boldsymbol{\nabla} \cdot \boldsymbol{B}' = 0. \tag{14}$$

This shows that Eq. (8) can be decoupled into two Floquet stability analyses: one for the hydrodynamic stability obtained through solving Eqs. (11) and (12) and another for the stability of the magnetic field through solving Eqs. (13) and (14). In other words, the hydrodynamic stability of the $\boldsymbol{U}_0$ flow is independent from the stability of the magnetic field. Hence we should expect that, in the kinematic regime, perturbations to the velocity and magnetic fields will grow independently of each other in accordance with their Floquet multipliers. It is important to note that this is the case only for a hydrodynamic basic state; decoupling would not occur for the Floquet stability of an MHD basic state. Although Floquet analysis around a periodic MHD state is also possible and would be relevant to the instability of saturated dynamo solutions to long wavelength instabilities, this is beyond the scope of our current paper.

Numerically, we solve the hydrodynamic and magnetic stability problems separately following the method discussed by Barkley and Henderson [20]. For the hydrodynamic stability problem, we let the state transition matrix for the linear problem given by Eqs. (11) and (12) be denoted by $\boldsymbol{\Psi}_U$. The action of $\boldsymbol{\Psi}_U(T)$ on a vector $\boldsymbol{a}$ is then provided in a matrix-free manner by solving Eqs. (11) and (12) with initial condition $\boldsymbol{U}' = \boldsymbol{a}$ over one period $T = 2\pi/\Omega$. The eigenvalues of $\boldsymbol{\Psi}_U(T)$ can then be found from this matrix-free operation using an eigenvalue solver, yielding the Floquet multipliers and modes. The magnetic stability problem is solved using the same procedure with Eqs. (13) and (14).

This procedure is achieved in Python by using the *linearOperator* functionality contained in the *linalg* module in the *scipy* library. This allows us to define a linear operator by providing a routine that defines a matrix-vector product. For us, this matrix-vector product is defined through using DEDALUS to solve the linear time-periodic equations, whose initial condition is the given vector, over one period. This linear operator can then be given to the *eigs* routine, a Python wrapper of the ARPACK library, also contained in the *linalg* module. In this manner, we can find the eigenvalues of the linear operator without explicitly constructing a matrix, i.e., only matrix-vector products are needed. Even though solving the PDE over one period each time the eigenvalue routine needs to evaluate a matrix-vector product is costly, the fact that the algorithm finds eigenvalues $\exp(\lambda_i T)$ that are largest in magnitude first means that in practice we naturally obtain eigenvalues for which the growth rate $\mathrm{Real}(\lambda_i)$ is largest. As these are the fastest growing modes which are physically the most important, this means that this approach is efficient and converges to the eigenvectors of interest without the need for a good initial guess.

C. Finite-time Lyapunov exponents

As noted in the Introduction, information about the degree of stretching in the flow can be gained by calculating the distribution of FTLEs. To calculate these, we follow the algorithm of Soward [21] (see also Ref. [22]) and consider tracking a set of particles that are passively advected by the fluid. Taking N particles with positions $\{\boldsymbol{p}_i\}_{i=0}^{N-1}$, we track the particles by solving

$$\frac{d}{dt}\boldsymbol{p}_i = \boldsymbol{U}(\boldsymbol{p}). \tag{15}$$

Letting $\mathcal{S}$ denote the fluid velocity gradient tensor with $\mathcal{S}(\boldsymbol{p}) = \boldsymbol{\nabla}_{\boldsymbol{x}=\boldsymbol{p}}\boldsymbol{U}$, we also solve

$$\frac{d}{dt}\boldsymbol{D} = \boldsymbol{S}(\boldsymbol{p})\boldsymbol{D} \tag{16}$$

for each particle path starting with $\boldsymbol{D} = \mathrm{diag}(2^{-1/2}, 2^{-1/2}, 0)$. For each time t, we form the matrix

$$\boldsymbol{C}(t) = \boldsymbol{D}(t)^T\boldsymbol{D}(t). \tag{17}$$

The FTLE connected to the position $\boldsymbol{x}_0$ is then the slope of $l(t;\boldsymbol{x}_0) = \ln(\sum_{i,j}\boldsymbol{C}_{i,j}(t)/2)/2$, where $\boldsymbol{C}$ arises from a particle whose initial position is $\boldsymbol{x}_0$. The slope of the line is found using linear regression.

When calculating the FTLEs, we solve the governing equations as described in the previous section, tracking the particles using a particle tracking code for DEDALUS developed for this paper. For what follows, we will concentrate on the calculation of FTLEs on the plane $z = 0$, i.e., the initial particle positions are taken to be equispaced $(x_i, y_i, 0)$, with the $x - y$ plane consisting of 128×128 particles and a time horizon of $T = 30$ matching that of Brummell *et al.* [15]. Due to the increased numerical burden of tracking the particles, the resolution is decreased to $64 \times 64 \times 64$ when calculating the FTLEs. However, the initial condition for tracking the particles always comes from the higher resolution results. This, coupled with the fact that the time horizon for the FTLE calculations is small, means that we stay close enough to the high resolution solution while keeping the computation feasible. The numerical code for particle tracking in DEDALUS V2 and FTLE calculation has been made available as part of the companion code for this paper [23].

D. Passive vector field evolution

A less rigorous, though still informative method for calculating the stretching properties of a flow is to calculate the response of a passive vector field to the flow. Following Cattaneo and Tobias [10], we will also consider the evolution of a passive vector field which satisfies the induction equation but does not couple with the velocity field via a Lorentz force. To this end, we solve Eqs. (1)–(3) together with

$$(\partial_t - \mathrm{Rm}^{-1}\nabla^2)\boldsymbol{Z} = \boldsymbol{\nabla} \times (\boldsymbol{U} \times \boldsymbol{Z}), \tag{18}$$

$$\boldsymbol{\nabla} \cdot \boldsymbol{Z} = 0. \tag{19}$$

By tracking $\boldsymbol{Z}$, we are able to see how a magnetic field would behave for the velocity field stemming from a nonlinearly saturated dynamo. While it seems that $\boldsymbol{Z}$, which solves the same equation as $\boldsymbol{B}$, must follow the same trajectory as $\boldsymbol{B}$, this is in fact only true if the initial condition for $\boldsymbol{Z}$ is the same as that of $\boldsymbol{B}$. The reason for this is that there is no $\boldsymbol{Z}$-based Lorentz force, meaning that $\boldsymbol{U}$ is independent of $\boldsymbol{Z}$ and that the evolution of $\boldsymbol{Z}$ is completely linear. As no particles are being tracked in this case, the resolution is again set at $96 \times 96 \times 96$. The aim here is to determine how well one can understand the chaotic properties of the flow using this proxy method, which is simpler (and less expensive) computationally than calculating the FTLEs.

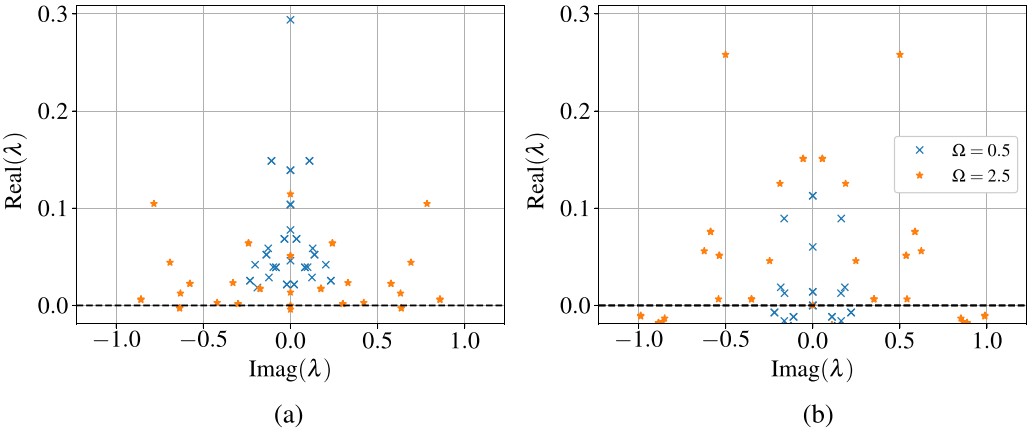

FIG. 2. Floquet exponents for $\epsilon = 1$, Re = Rm = 100. The stability boundary is shown as a dotted line in each figure (a) Hydrodynamic Floquet exponents and (b) Magnetic Floquet exponents.

III. RESULTS

A. Floquet stability analysis

We begin our results by considering the stability of the periodic state $\boldsymbol{U}_0$, using the procedure outlined in Sec. II B. Again, we stress that around a purely hydrodynamic base state, the hydrodynamic and magnetic stability problems decouple and may be considered separately. Figure 2 shows the Floquet exponents found for the two cases at two representative frequencies. For Floquet exponents λ with Real(λ) > 0, there will be an exponential growth of the mode, indicating instability. Hence, exponents above the line Real(λ) $= 0$ indicate unstable directions.

For Re = Rm = 100 the flow is, in general, more unstable to magnetic perturbations rather than hydrodynamic perturbations, agreeing with the observations of Brummell *et al.* [15]. However, for $\Omega = 0.5$ this is not the case and the flow is much more unstable to a hydrodynamic perturbation with Imag(λ) $= 0$, which shows that it is a purely growing instability and has no oscillation frequency associated with it. This is made clearer by considering the maximum growth rate for each frequency, displayed in Fig. 3.

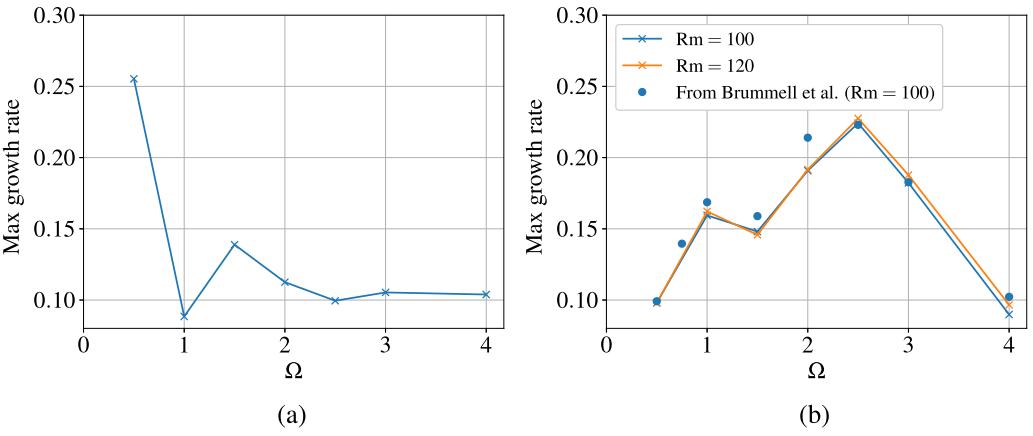

FIG. 3. Maximum growth rates for the hydrodynamic and magnetic stability problems (a) Maximum growth rates for the kinetic energy and (b) Maximum growth rates for the magnetic energy.

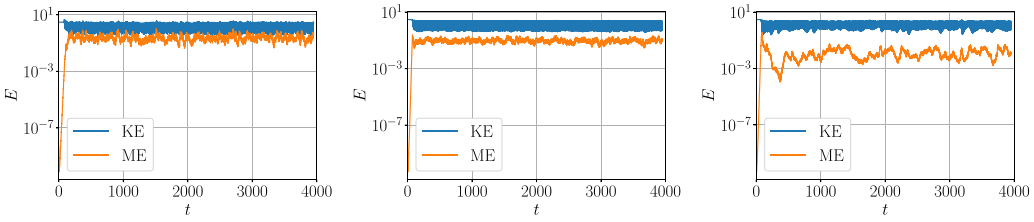

(a) $\Omega = 0.5$ (b) $\Omega = 1.0$ (c) $\Omega = 1.5$

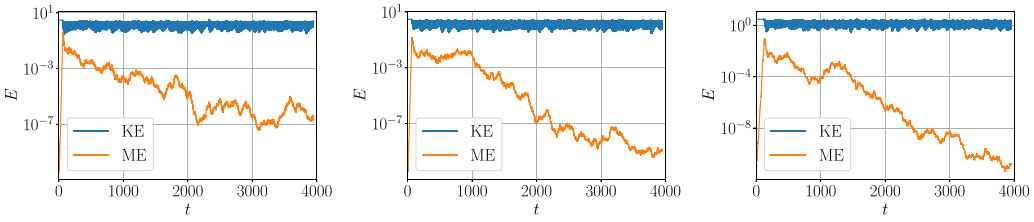

(d) $\Omega = 2.0$ (e) $\Omega = 3.0$ (f) $\Omega = 4.0$

FIG. 4. Kinetic and magnetic energies over time for $\epsilon = 1$, $\mathrm{Re} = 100$, and $\mathrm{Rm} = 100$, starting from a small magnetic perturbation and a velocity field in $\boldsymbol{U}_0$.

For verification of our Floquet approach, the results of Brummell *et al.* [15] are added to Fig. 3(b). As we can see, there is a good quantitative agreement with our results bounded above by those of Brummell *et al.* [15]. The reason for this can be attributed to the method used to obtain the growth rates. Ours stem from a single modal structure, whereas those of Brummell *et al.* [15] are obtained via linear regression of the magnetic energy obtained from a simulation, meaning that the superposition of two or more growing modes can give rise to a higher magnetic energy growth rate. Figure 3 also shows the results of the Floquet analysis at $\mathrm{Rm} = 120$. As the maximum growth rate does not change significantly, we can postulate that we are in a regime where the growth rate has saturated as a function of Rm; in this sense, the time-dependent flows are acting asquick dynamos [17]. This asymptotic behavior is believed to set in at lower magnetic Reynolds numbers for time-varying hydrodynamic states [6,15], than for steady ABC flow [24].

B. Nonlinear evolution

Before considering the FTLEs, we first summarize the flow behavior of an initial state consisting of a small magnetic field and the hydrodynamic state $\boldsymbol{U}_0$. Figure 4 shows the results for $\mathrm{Re} = \mathrm{Rm} = 100$. We see that for all frequencies there is an initial exponential growth of the magnetic field. This is not surprising, as the results of the Floquet analysis show that the flow is unstable to magnetic perturbations. More interesting is the subsequent behavior. For the considered frequencies $\Omega \leqslant 1.5$, the magnetic energy saturates, showing that the Lorentz force acts to stabilze the growth of the magnetic field. However, for higher frequencies the magnetic energy eventually decays. This means that the velocity field that results after deviation from its initial $\boldsymbol{U}_0$ form is stable to magnetic perturbations. In this case, the magnetic energy eventually decays to negligible values, leaving a purely hydrodynamic state. We note that as, at the Reynolds numbers considered, the state $\boldsymbol{U}_0$ is unstable (see Sec. III A), this secondary hydrodynamic state can also be reached from a hydrodynamic simulation via the instability of the base state to hydrodynamic perturbations. In other words, the magnetic field is not essential in reaching this state, but can cause it to not appear in cases where a nonlinear dynamo is produced. Following Brummell *et al.* [15], we call this secondary purely hydrodynamic state, seen for $\Omega \geqslant 2$ when the magnetic field is negligible, $\boldsymbol{U}_1$. When the magnetic field does not decay, we do not reach $\boldsymbol{U}_1$ but instead a joint MHD state.

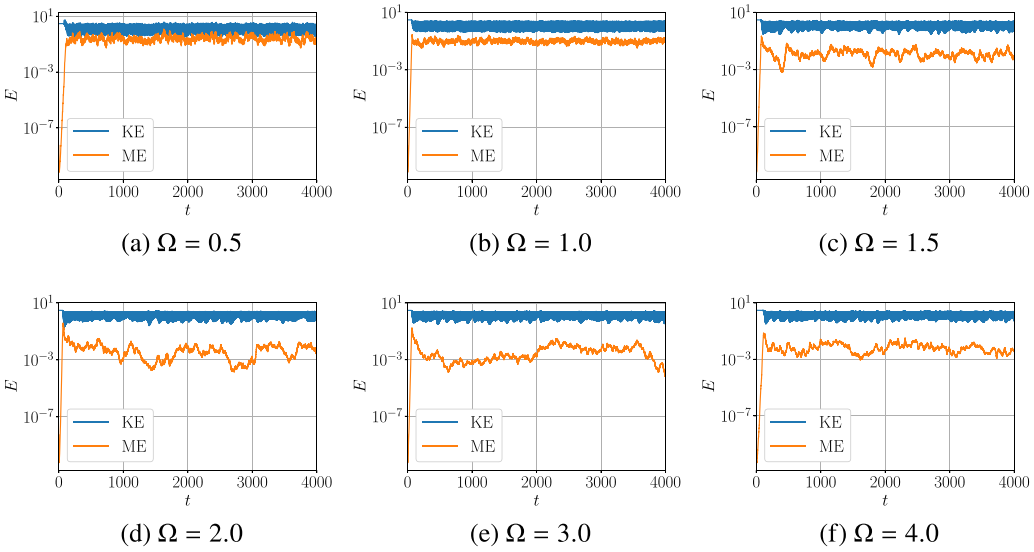

(a) $\Omega = 0.5$ (b) $\Omega = 1.0$ (c) $\Omega = 1.5$

(d) $\Omega = 2.0$ (e) $\Omega = 3.0$ (f) $\Omega = 4.0$

FIG. 5. Kinetic and magnetic energies over time for $\epsilon = 1$, $\mathrm{Re} = 100$, and $\mathrm{Rm} = 120$, starting from a small magnetic perturbation and a velocity field in $\boldsymbol{U}_0$.

Repeating this procedure at the higher magnetic Reynolds number of $\mathrm{Rm} = 120$, we obtain Fig. 5. In this case, for all frequencies the dynamo saturates, leading to a nonlinear dynamo solution. As the Floquet analysis revealed that there is no significant change in the stability properties of $\boldsymbol{U}_0$ for $\mathrm{Rm} = 120$, the reason behind this saturation must either lie in the stability properties of $\boldsymbol{U}_1$ to magnetic perturbations or in nonlinear interactions between the magnetic field and velocity field via the Lorentz force. Hence, to investigate this we examine the stability properties of $\boldsymbol{U}_1$.

As $\boldsymbol{U}_1$ is not an exact periodic solution of the governing equations but is instead a quasiperiodic state, we cannot use Floquet theory to determine the behavior of a small magnetic field. Instead we run a simulation starting from an initial state in the $\boldsymbol{U}_1$ attractor and seed it with a small random magnetic field. The results of this for $\mathrm{Rm} = 100$ and $\mathrm{Rm} = 120$ are shown in Figs. 6 and 7, respectively. For $\mathrm{Rm} = 100$, Fig. 6 shows that the frequencies at which the magnetic energy eventually decays are the same frequencies at which $\boldsymbol{U}_1$ is stable to magnetic perturbations. This means that if nonlinear effects are unable to alter the velocity field, then the magnetic field will eventually decay with no chance to grow again. For this reason, at $\mathrm{Re} = 100$ where the hydrodynamic state $\boldsymbol{U}_0$ is unstable, it is unclear whether these dynamos are self-killing initially through an unfavorable modification of the velocity field via the Lorentz force or whether they decay through the rise of the stable $\boldsymbol{U}_1$ hydrodynamic state. It is also worth noting that although the other frequencies are unstable to magnetic perturbations, the growth rates are significantly reduced than that obtained for $\boldsymbol{U}_0$, indicating that while $\boldsymbol{U}_1$ is still susceptible to kinematic dynamo action, it is less efficient. For all frequencies Ω in which the magnetic field grows, we will eventually reach the same nonlinear dynamo solution achieved more efficiently when starting from $\boldsymbol{U}_0$.

Turning our attention to $\mathrm{Rm} = 120$, we see from Fig. 7 that all frequencies show a positive growth rate. However, for $\Omega \geqslant 2$ this growth rate is extremely small, with $\Omega = 2.5$ not rising significantly on a long timescale. Therefore, on short timescales the flow will appear neutral to magnetic perturbations and we can expect that only a slight nonlinear effect via the Lorentz force will be needed to saturate the growth of magnetic energy. Again we note that for all frequencies, the growth rates for $\boldsymbol{U}_1$ are lower than that of $\boldsymbol{U}_0$.

We conclude this section by summarizing the possible states observed for our system sketched in Fig. 8. The first state is that of $\boldsymbol{U}_0$ defined through Eq. (4). This state is hydrodynamically

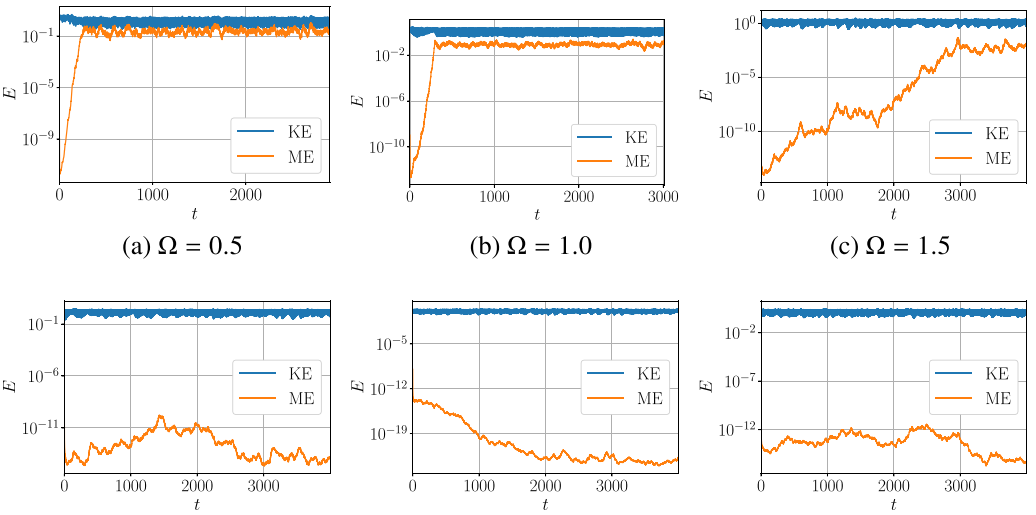

(a) $\Omega = 0.5$ (b) $\Omega = 1.0$ (c) $\Omega = 1.5$

(d) $\Omega = 2.0$ (e) $\Omega = 2.5$ (f) $\Omega = 4.0$

FIG. 6. Kinetic and magnetic energies over time for $\epsilon = 1$, Re $= 100$, and Rm $= 100$ starting from a small magnetic perturbation and a velocity field in $\boldsymbol{U}_1$.

unstable, as shown in Sec. III A, and hence a purely hydrodynamic simulation starting from $\boldsymbol{U}_0$ will lead to a second new quasiperiodic hydrodynamic state termed $\boldsymbol{U}_1$ following Ref. [15]. As the results of the Floquet analysis confirm that $\boldsymbol{U}_0$ is much more unstable to magnetic rather than hydrodynamic perturbations, introducing a small magnetic field leads to kinematic dynamo action on a timescale in which the velocity field does not deviate from its unstable $\boldsymbol{U}_0$ configuration. This kinematic dynamo action can lead to two distinct possibilities dependent upon the magnetic Reynolds number Rm and frequency Ω. One is that the Lorentz force modifies the velocity field

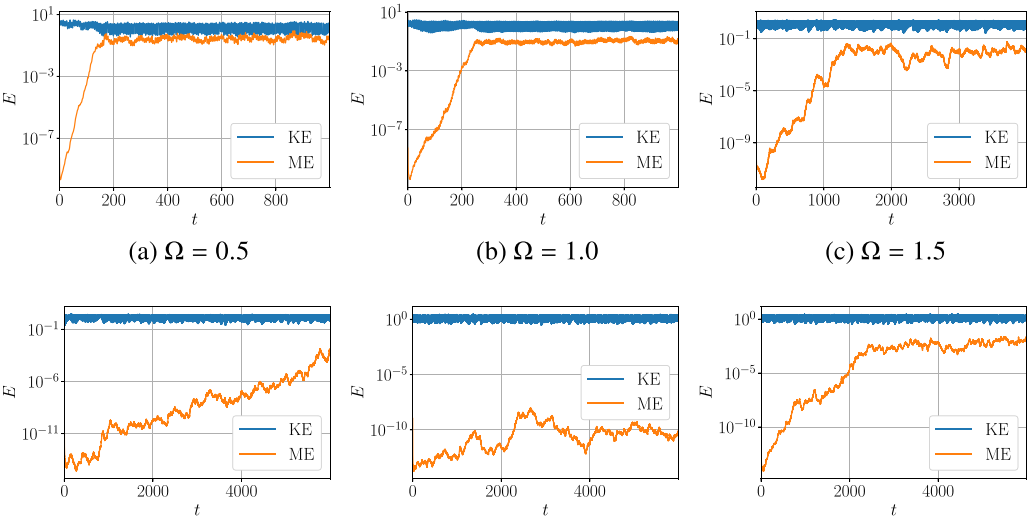

(a) $\Omega = 0.5$ (b) $\Omega = 1.0$ (c) $\Omega = 1.5$

(d) $\Omega = 2.0$ (e) $\Omega = 2.5$ (f) $\Omega = 4.0$

FIG. 7. Kinetic and magnetic energies over time for $\epsilon = 1$, Re $= 100$, and Rm $= 120$ starting from a small magnetic perturbation and a velocity field in $\boldsymbol{U}_1$.

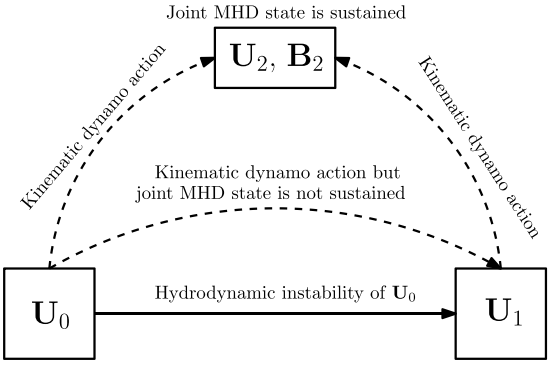

FIG. 8. Sketch summarizing the various states of interest as well as the possible paths between them. The dashed line represents paths that are dependent on the magnetic Reynolds number Rm and frequency Ω. The solid line shows a purely hydrodynamic pathway that always occurs at the Reynolds number in this paper.

leading to an MHD state, denoted $\boldsymbol{U}_2$, $\boldsymbol{B}_2$ in Fig. 8. The second is that there is kinematic dynamo action but a self-sustaining MHD state does not occur, leading to the eventual decay of the magnetic field leaving the hydrodynamic state $\boldsymbol{U}_1$. In the cases where $\boldsymbol{U}_1$ is unstable to magnetic perturbations kinematic dynamo action is also possible by seeding $\boldsymbol{U}_1$ with a small magnetic field. The amplifies until saturation leads to the MHD state $\boldsymbol{U}_2$, $\boldsymbol{B}_2$.

C. Lagrangian statistics

Now that the nonlinear evolution of a magnetic field has been described for a range of parameters, we turn our attention to understanding the growth and saturation of the magnetic field via an examination of the Lagrangian statistics of the flow field. We first seek to verify the particle tracking code with the work of Brummell *et al.* [15]. To this end, we set $\mathrm{Re} = 100$, $\mathrm{Rm} = 100$, $\epsilon = 1$ and consider a range of values for Ω on the plane $z = 0$. For these parameters the flow field $\boldsymbol{U}$ remains close to $\boldsymbol{U}_0$ despite the exponentially growing magnetic field due to the stability properties of the hydrodynamic state (see Sec. III A). This means that by calculating the FTLEs with a time integration of 30 time-units, we stay within this kinematic regime and our results should match those of Brummell *et al.* [15] for which the $\boldsymbol{U}_0$ flow is imposed.

Figure 9(a) shows the mean FTLEs calculated with our current approach and with the results of Brummell *et al.* [15]. We see that the calculated values show good agreement, both verifying our approach and showing that the results of Brummell *et al.* [15] hold in the presence of a small, but nonzero, magnetic field. The weak field here has had very little impact on the degree of chaos in the flow. As in Ref. [15], we see that there is a qualitative correspondence between the mean FTLEs and the stability properties of $\boldsymbol{U}_0$. Indeed, larger values of the FTLE occur at frequencies for which the magnetic growth rate [shown in Fig. 3(b)] is highest.

Having verified our particle tracking approach, we now consider calculating the FTLEs for the secondary hydrodynamic state $\boldsymbol{U}_1$. Figure 9(b) shows that the flow $\boldsymbol{U}_1$ is on average less chaotic than $\boldsymbol{U}_0$ with the FTLEs for most frequencies decreasing. The exception to this is the lowest frequency considered, $\Omega = 0.5$. For this frequency, the mean FTLE for $\boldsymbol{U}_1$ is significantly greater than for $\boldsymbol{U}_0$. One possible explanation for this can be obtained by examining the stability of $\boldsymbol{U}_0$ to hydrodynamic perturbations. There are two main reasons for suspecting this link. The first is that there is a correspondence between the maximum growth rates of the kinetic energy [shown in Fig. 3(a)] and the mean FTLEs of $\boldsymbol{U}_1$, where the maximum in both cases is found for $\Omega = 0.5$ with relatively flat behavior for all other frequencies. The second is that there are more unstable directions for $\Omega = 0.5$ than for all other frequencies. Hence, it seems plausible that the increased propensity to hydrodynamic instability for $\Omega = 0.5$ could lead to a more chaotic flow.

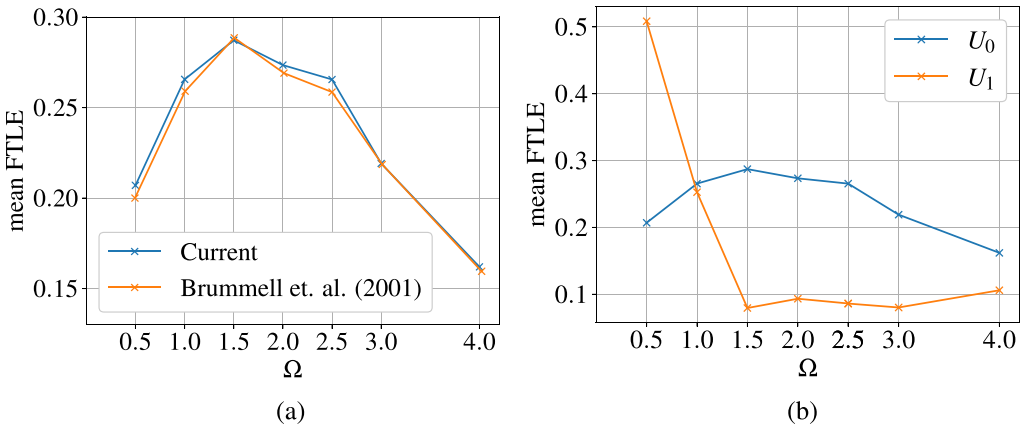

FIG. 9. Mean FTLEs for $\boldsymbol{U}_0$ and $\boldsymbol{U}_1$ for a range of values of Ω and $\epsilon = 1$ at $\mathrm{Re} = 100$ (a) Mean FTLEs for U_0 using an MHD code in the kinematic regime with $\mathrm{Rm} = 100$. Also shown are the results of Brummell *et al.* [9] for comparison and (b) Mean FTLEs for U_1 calculated with a purely hydrodynamic simulation. The results for U_0 are also shown.

Before moving on to cases with a magnetic field present, we examine the structure of the FTLEs on the plane $z = 0$ for our two hydrodynamic states. Given that we have just shown that the FTLEs do not differ significantly from purely kinematic results in which the flow $\boldsymbol{U}_0$ is specified, we present results for $\boldsymbol{U}_0$, obtained from a code that fixes the velocity field, at a higher resolution than is feasible for our other cases in Fig. 10. The figure shows that for all frequencies the flow is quite chaotic with very few integrable patches (indicated by dark regions). We note that the ridges present in these figures are related to Lagrangian coherent structures and act as barriers through which particle paths do not cross [26,27].

The FTLEs for $\boldsymbol{U}_1$ are displayed in Fig. 11. It is immediately clear that the Lagrangian statistics are quite different from that of $\boldsymbol{U}_0$. For low frequencies, in which the mean FTLEs increase or remain similar, we see that the flow remains chaotic nearly everywhere. This is especially evident for $\Omega = 0.5$, which shows very little areas of integrability. However, for the frequencies where the mean FTLEs decrease the areas of integrability are substantially larger, with thin ridges separating them. These changes from $\boldsymbol{U}_0$ reflected in the structure, and mean, of the FTLEs shows that as for $\boldsymbol{U}_0$ there is a clear link between the FTLEs and the magnetic energy growth rates for $\boldsymbol{U}_1$ (discussed in Sec. III B).

It is important to note that, although the FTLE for $\Omega = 0.5$ is higher for $\boldsymbol{U}_1$ than $\boldsymbol{U}_0$, the growth rate is smaller. This reminds us that care is needed when interpreting the FTLEs and that formally the link between the growth rate of a magnetic field and the FTLEs is obtained for $\mathrm{Rm} \to \infty$. However, for $\boldsymbol{U}_0$ we see from our Floquet results that it may be a quick dynamo, setting into this asymptotic fast dynamo behavior at our current parameters. Therefore, the discrepancy for $\boldsymbol{U}_1$ suggests that we have simply not reached this asymptotic behavior (if, in fact, it exists).

With the hydrodynamic behavior discussed, let us turn our attention to cases in which a magnetic field is present. For $\mathrm{Rm} = 100$, Sec. III B showed that, unlike for $\mathrm{Rm} = 120$, not all frequencies have a region in which a nonlinear dynamo is sustained. Therefore, we calculate the FTLEs starting from states at a few points in the region where the kinematic growth phase has ended, but before the eventual decay of the magnetic field. For $\mathrm{Rm} = 120$, a nonlinear dynamo is sustained at all frequencies, hence we start the FTLE calculation from a representative state in the nonlinear regime.

Figures 12(a) and 12(b) show the mean FTLE for $\mathrm{Rm} = 100$ and $\mathrm{Rm} = 120$, respectively. From Fig. 12(a), we see that the mean FTLE does not depend strongly on the state at which the calculation is started. The slight variations can therefore be mainly attributed to the natural slight variation that can be expected when starting the FTLE calculation from a different point of the attractor. For low

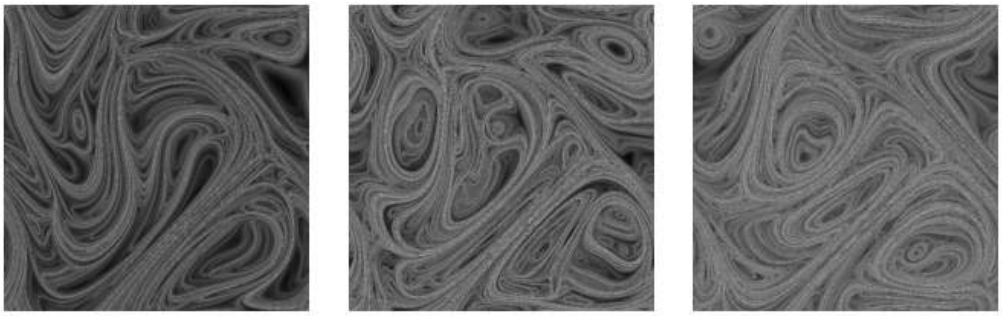

(a) $\Omega = 0.5$ (b) $\Omega = 1.0$ (c) $\Omega = 1.5$

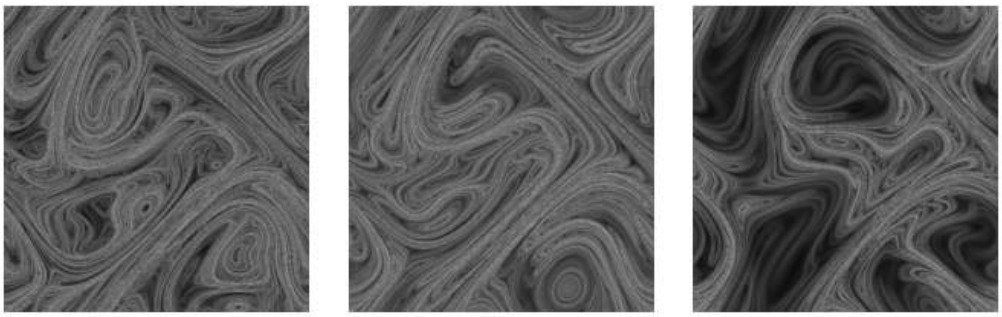

(d) $\Omega = 2.0$ (e) $\Omega = 2.5$ (f) $\Omega = 4.0$

FIG. 10. FTLEs in the kinematic regime with $\epsilon = 1$. A greyscale color map is used, with a FTLE of zero being black and the maximum FTLE being white. Movies of their evolution over five periods are available as Supplemental Material [25].

frequencies, the mean FTLE of the nonlinear state is different from that of $\boldsymbol{U}_1$ [shown in Fig. 12(b)]. This indicates that the Lorentz force is large enough that is has significantly altered the flow field from its $\boldsymbol{U}_1$ form. However, for higher frequencies the mean FTLEs are close to that of $\boldsymbol{U}_1$, showing that no such flow modification is taking place, leading to the eventual decay of the magnetic field.

For $\mathrm{Rm} = 120$, we see from Fig. 12(b) a similar pattern to that obtained for $\mathrm{Rm} = 100$. It is clear that for $\Omega = 0.5$ and $\Omega = 1.0$ that the Lorentz force is significantly altering the flow field, leading to lower FTLEs and a less chaotic flow in the nonlinear dynamo regime. However, for higher frequencies there is an overall agreement for the mean FTLE in the nonlinear regime and for the hydrodynamic state $\boldsymbol{U}_1$. As in these cases the flow remains a nonlinear dynamo, despite not significantly modifying the purely hydrodynamic flow, it is reasonable to suspect that the marginal instability of $\boldsymbol{U}_1$ to magnetic perturbations (shown in Sec. III B) is partially responsible for its saturation. The FTLEs for $\mathrm{Rm} = 120$ on the plane $z = 0$ are shown in Fig. 13. These FTLE images support the findings of the mean FTLEs, namely, that for $\Omega = 0.5$ and $\Omega = 1.0$ the flow is less chaotic than $\boldsymbol{U}_1$ (see Fig. 11), but has no noticeable difference from $\boldsymbol{U}_1$ for other frequencies.

To provide clearer evidence for whether the magnetic field is altering the FTLEs, we can consider the PDFs of the FTLEs. For this purpose, we consider two frequencies: $\Omega = 0.5$, for which the mean FTLE is altered, and $\Omega = 2.5$, which shows little difference. For both frequencies, a normal distribution is found to be a good fit, with the resulting PDFs shown in Fig. 14. For $\Omega = 0.5$, Fig. 14(a) shows that there us a clear difference in the distribution of the FTLEs between $\boldsymbol{U}_0$ and $\boldsymbol{U}_1$, with the flow becoming more chaotic in $\boldsymbol{U}_1$ and any integrable regions present for $\boldsymbol{U}_0$ disappearing. Importantly, we see that the distribution for the nonlinear dynamo is between that of $\boldsymbol{U}_0$ and $\boldsymbol{U}_1$.

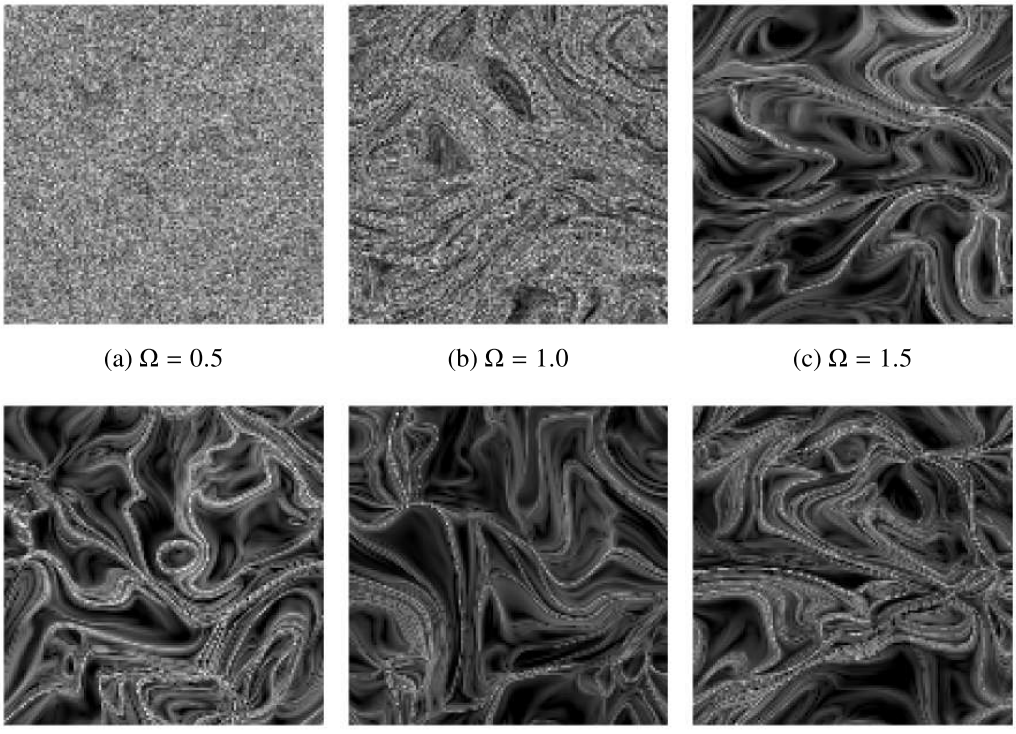

(a) $\Omega = 0.5$ (b) $\Omega = 1.0$ (c) $\Omega = 1.5$

(d) $\Omega = 2.0$ (e) $\Omega = 2.5$ (f) $\Omega = 4.0$

FIG. 11. FTLEs for $\boldsymbol{U}_1$ with $\mathrm{Re} = 100$ and $\epsilon = 1$. A greyscale color map is used, with a FTLE of zero being black and the maximum FTLE being white.

Therefore, it is clear that the Lorentz force is playing a major role in this case, preventing the emergence of a $\boldsymbol{U}_1$-type flow, and modifying the velocity field to an overall less chaotic one (than $\boldsymbol{U}_1$—though this is still more chaotic than $\boldsymbol{U}_0$).

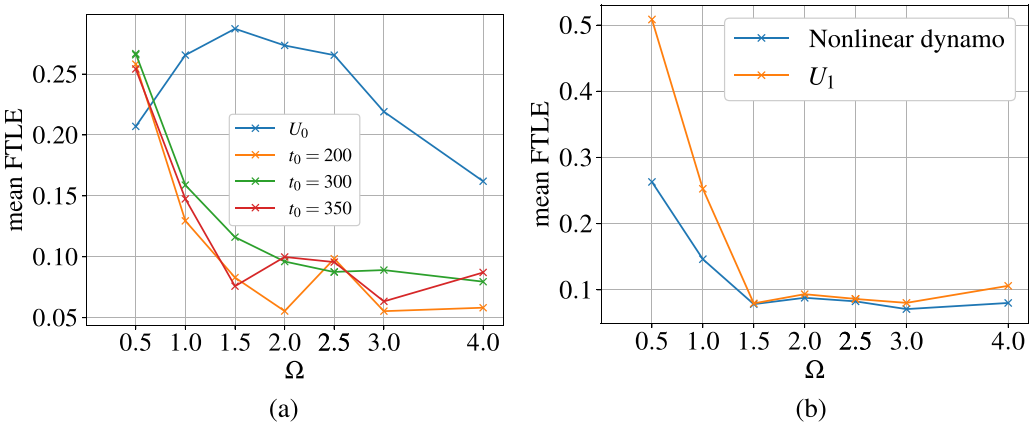

FIG. 12. Mean FTLEs for a range of frequencies with $\mathrm{Re} = 100$ and $\epsilon = 1$ (a) Mean FTLEs for the nonlinear regime at $\mathrm{Rm} = 100$ and (b) Mean FTLEs for the nonlinear regime at $\mathrm{Rm} = 120$.

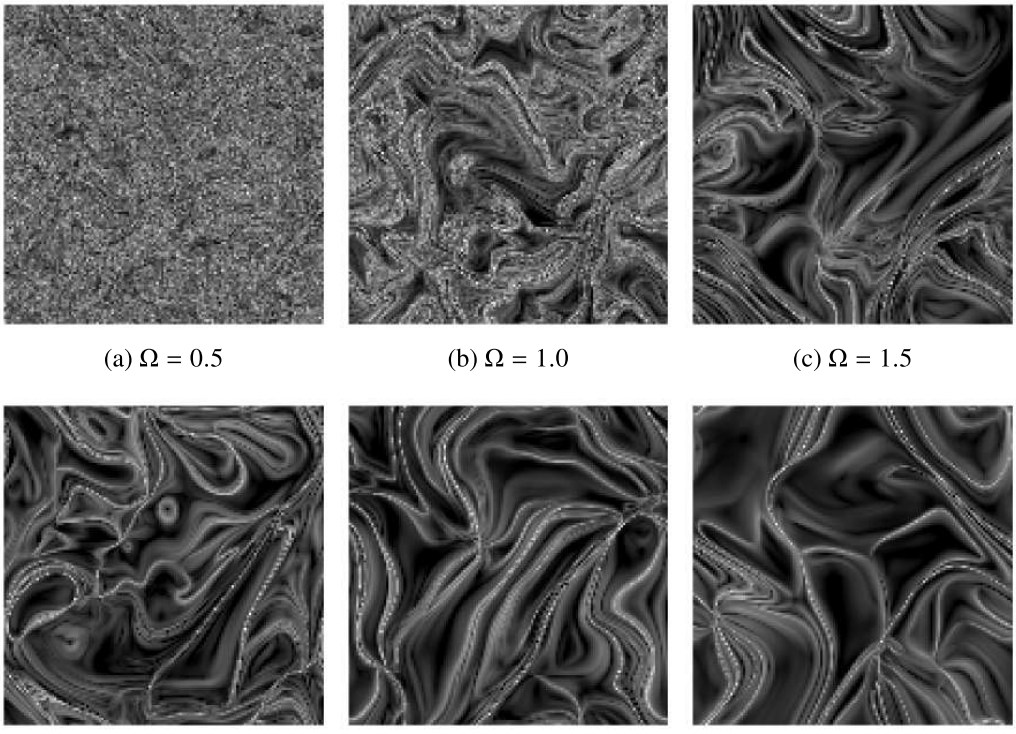

(a) $\Omega = 0.5$ (b) $\Omega = 1.0$ (c) $\Omega = 1.5$

(d) $\Omega = 2.0$ (e) $\Omega = 2.5$ (f) $\Omega = 4.0$

FIG. 13. FTLEs in the nonlinear regime with $\mathrm{Re} = 100$, $\mathrm{Re} = 120$, and $\epsilon = 1$. A grayscale color map is used, with a FTLE of zero being black and the maximum FTLE being white.

Conversely, Fig. 14(b) shows seemingly identical distributions for $\boldsymbol{U}_1$ and the nonlinear dynamo regime. This supports the hypothesis that the Lorentz force is doing very little to modify the velocity field for $\Omega = 2.5$. The reason then for saturation of the dynamo can mainly be attributed

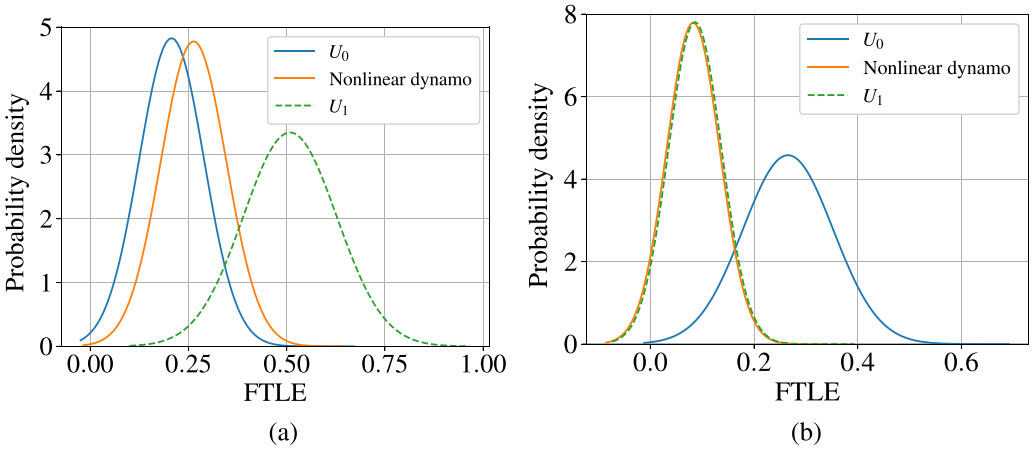

FIG. 14. Probability density function of the FTLEs at $\mathrm{Rm} = 120$. (a) $\Omega = 0.5$ and (b) $\Omega = 2.5$.

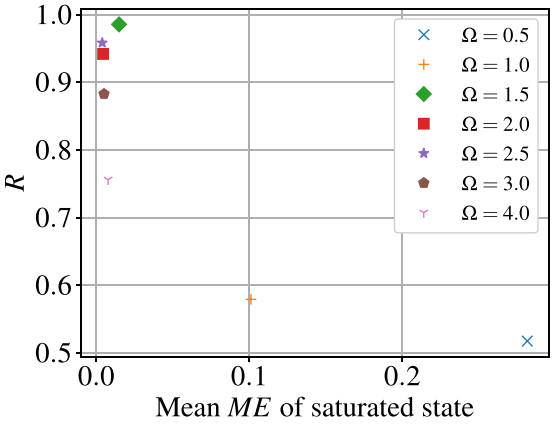

FIG. 15. The ratio of the mean FTLE of the nonlinear dynamo for Rm = 120 to the mean FTLE of the $\boldsymbol{U}_1$ state (R) versus the mean ME of the saturated solution.

to the marginal (almost neutral) instability to magnetic perturbations properties of $\boldsymbol{U}_1$ at $\Omega = 2.5$. Therefore, even though the magnetic field must influence the velocity field to saturate, it need only do so very weakly and on long timescales. Hence, the nonlinear dynamo regime can have a velocity field that remains close to $\boldsymbol{U}_1$. In general, Fig. 15 illustrates that the mean-field strength of the dynamo is anticorrelated with the agreement between the mean FTLEs of the nonlinear dynamo and the hydrodynamic state $\boldsymbol{U}_1$. This indicates that the frequencies at which the magnetic field strength is lower ($\Omega \geqslant 1.5$) are the same as those for which the nonlinear dynamo has the same chaotic properties as $\boldsymbol{U}_1$.

D. Passive kinematic dynamo

We conclude the results by examining the stability properties of a passive vector field, governed by Eq. (18). By time stepping this passive dynamo in the flow field of the nonlinear dynamo regime, we can see whether the flow field remains able to amplify a kinematic vector field despite dynamo saturation. The evolution of $\boldsymbol{Z}$ starting from a small random initial condition is shown in Fig. 16. From Fig. 16(a), we see that only $\Omega = 0.5$ has a significantly positive growth, with all other cases being only slightly positive or negative. This is further highlighted by the growth rates illustrated in Fig. 16(b). From these results, we can see that, as in Ref. [10], the flow field from a saturated nonlinear dynamo can remain a kinematic dynamo. The reason for this can be related to the correspondence between the growth rates of Fig. 16(b) and the mean FTLEs [Fig. 12(b)], again highlighting the link between the FTLEs of a flow field and the kinematic growth rate of a magnetic field as conjectured by Cattaneo and Tobias [10]. Hence, calculating the evolution of a passive vector field is a good proxy for a full Lagrangian calculation.

As for $\Omega = 0.5$, the passive scalar dynamo is unstable—it shows that the form of the magnetic field and its link to the velocity field is crucial in providing saturation in this case. In other words, although kinematic growth is possible, as suggested by the FTLEs, nonlinear growth is not due to the way in which the velocity and magnetic fields nonlinearly interact. Hence, it can be thought that for nonlinear regimes with more chaotic properties, nonlinearity is crucial in providing saturation, and the flow field must be significantly modified via the Lorentz force. For the other frequencies, the growth rate is smaller and we should not read too much into their exact values. Indeed, the results of Sec. III B show that very small growth rates for the magnetic field are possible on a timescale not considered for the passive dynamo. Instead, as the flow remains close to $\boldsymbol{U}_1$, we should expect that the passive scalar dynamo, although eventually increasing as it should for $\boldsymbol{U}_1$ (Fig. 7), can have

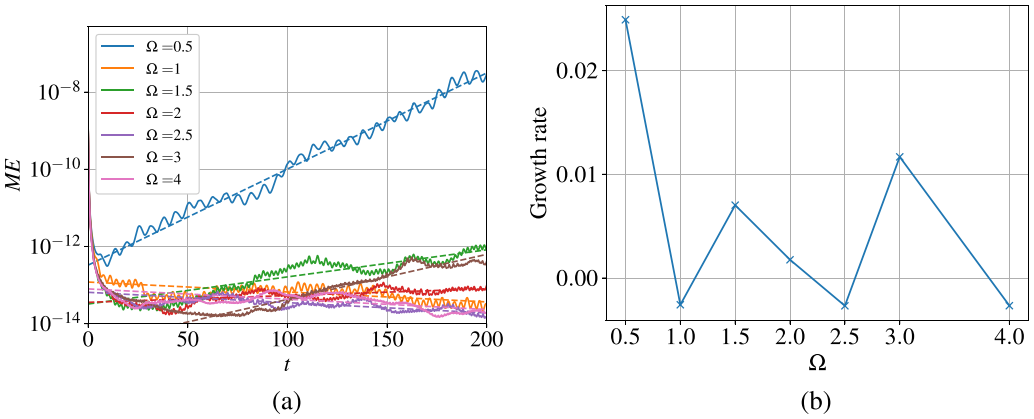

FIG. 16. Magnetic energy evolution and growth rates for a passive kinematic dynamo $\boldsymbol{Z}$ in the nonlinear regime for $\mathrm{Rm} = 120$ (a) Magnetic energy evolution for a range of frequencies Ω and (b) Growth rates obtained by linear regression of the magnetic energy time series [shown as dotted lines in (a)].

local periods of stability as shown in Fig. 16(b). These local areas of stability could result from a weak Lorentz force and are enough to saturate the flow.

IV. CONCLUSION

In this paper, we have revisited the dynamo properties of a class of periodic (in space) oscillatory dynamo flows for a range of oscillation frequencies and fluids and magnetic Reynolds numbers. We have calculated the stability of such flows, both to hydrodynamic and magnetic perturbations using a Floquet analysis. Furthermore, we have examined the Lagrangian stretching properties of the kinematic and saturated dynamo flows, using a particle tracking method that enables the calculation (in the open source software DEDALUS) of the FTLEs [23]. We find that, depending on the frequency of oscillation, the stretching in the saturated state as measured by the average FTLE may increase or (more usually) decrease. The distribution of FTLEs remains well-approximated by a normal distribution in the saturated regime though the mean and variance of this distribution is modified by the presence of the magnetic field.

We further demonstrate that the calculation of the evolution of a passive vector field gives a very good proxy for a full Lagrangian calculation, validating the approach taken by Cattaneo and Tobias [10]. Interestingly, Cattaneo and Tobias [10] found cases in both convecting systems and forced shell models where the growth rate of a passively stretched vector field for a saturated dynamo state *increased* from that for the hydrodynamic velocity field. This was the case for a subset of the forced models considered here—confirmed via calculation of the FTLEs. Hence, it is not simple to predict *a priori* whether the presence of a magnetic field in the saturated state will lead to the diminution of chaos. It remains an interesting avenue for future investigation when the structure of dynamo flows and the generated magnetic field does lead to a system with increased stretching and chaos.

There are certainly systems where such an increase in chaos and turbulence is believed to be significant. For example, in essentially nonlinear dynamos, a finite amplitude magnetic field can lead to the onset of turbulence and hence chaotic stretching. Such dynamos are often subcritical and we conjecture that subcriticality may sometimes be associated with an increase of chaotic stretching imparted by the change in stability provided by a finite amplitude magnetic field.

Finally, we note that the Floquet analysis we perform here about the hydrodynamic state is particularly simple, as it separates into two independent classes of modes. The case of Floquet analysis about a saturated MHD state is more complicated. This case is relevant in determining the stability of saturated MHD states to long wavelength instabilities (see Ref. [28], for example) and

hence the important problem of the generation of large-scale magnetic field from a fully saturated small-scale dynamo.

ACKNOWLEDGMENTS

This work was undertaken on ARC4, part of the High Performance Computing facilities at the University of Leeds, UK. We acknowledge partial support from a grant from the Simons Foundation (Grant No. 662962, GF). We would also like to acknowledge support of funding from the European Union Horizon 2020 research and innovation program (Grant Agreement No. D5S-DLV-786780). Additionally, we would like to thank the Isaac Newton Institute for Mathematical Sciences, Cambridge, for support and hospitality during the programme DYT2 where work on this paper was undertaken. This work was supported by EPSRC Grant No. EP/R014604/1.

[1] K. Moffatt and E. Dormy, *Self-Exciting Fluid Dynamos*, Cambridge Texts in Applied Mathematics (Cambridge University Press, Cambridge, 2019).
[2] I. Klapper and L. S. Young, Rigorous bounds on the fast dynamo growth-rate involving topological entropy, Commun. Math. Phys. **173**, 623 (1995).
[3] J. M. Finn and E. Ott, Chaotic flows and fast magnetic dynamos, Phys. Fluids **31**, 2992 (1988).
[4] A. Brandenburg and K. Subramanian, Astrophysical magnetic fields and nonlinear dynamo theory, Phys. Rep. **417**, 1 (2005).
[5] F. Cattaneo and S. I. Vainshtein, Suppression of turbulent transport by a weak magnetic field, Astrophys. J. **376**, L21 (1991).
[6] S. M. Tobias, The turbulent dynamo, J. Fluid Mech. **912**, P1 (2021).
[7] A. V. Gruzinov and P. H. Diamond, Self-Consistent Theory of Mean-Field Electrodynamics, Phys. Rev. Lett. **72**, 1651 (1994).
[8] E. G. Blackman and G. B. Field, Constraints on the magnitude of α in dynamo theory, Astrophys. J. **534**, 984 (2000).
[9] F. Cattaneo, G. Bodo, and S. M. Tobias, On magnetic helicity generation and transport in a nonlinear dynamo driven by a helical flow, J. Plasma Phys. **86**, 905860408 (2020).
[10] F. Cattaneo and S. M. Tobias, Dynamo properties of the turbulent velocity field of a saturated dynamo, J. Fluid Mech. **621**, 205 (2009).
[11] F. Cattaneo, D. W. Hughes, and E.-J. Kim, Suppression of Chaos in a Simplified Nonlinear Dynamo Model, Phys. Rev. Lett. **76**, 2057 (1996).
[12] E. Zienicke, H. Politano, and A. Pouquet, Variable Intensity of Lagrangian Chaos in the Nonlinear Dynamo Problem, Phys. Rev. Lett. **81**, 4640 (1998).
[13] E. L. Rempel, A. C-L Chian, and A. Brandenburg, Lagrangian chaos in an ABC-forced nonlinear dynamo, Phys. Scr. **86**, 018405 (2012).
[14] H. Homann, Y. Ponty, G. Krstulovic, and R. Grauer, Structures and Lagrangian statistics of the Taylor-Green dynamo, New J. Phys. **16**, 075014 (2014).
[15] N. H. Brummell, F. Cattaneo, and S. M. Tobias, Linear and nonlinear dynamo properties of time-dependent ABC flows, Fluid Dyn. Res. **28**, 237 (2001).
[16] B. Galanti, A. Pouquet, and P. Sulem, Influence of the period of an ABC flow on its dynamo action, in *Solar and Planetary Dynamos*, Publications of the Newton Institute, edited by M. R. E. Proctor, P. C. Matthews, and A. M. Rucklidge (Cambridge University Press, Cambridge, 1994), pp. 99–104.
[17] S. M. Tobias and F. Cattaneo, Dynamo action in complex flows: The quick and the fast, J. Fluid Mech. **601**, 101 (2008).
[18] G. Floquet, Sur les équations différentielles linéaires à coefficients périodiques, Ann. Sci. Ec. Norm. Super. **12**, 47 (1883).

[19] K. J. Burns, G. M. Vasil, J. S. Oishi, D. Lecoanet, and B. P. Brown, Dedalus: A flexible framework for numerical simulations with spectral methods, Phys. Rev. Res. **2**, 023068 (2020).
[20] D. Barkley and R. D. Henderson, Three-dimensional Floquet stability analysis of the wake of a circular cylinder, J. Fluid Mech. **322**, 215 (1996).
[21] A. M. Soward, Fast dynamos, in *Lectures on Solar and Planetary Dynamos*, Publications of the Newton Institute, edited by M. R. E. Proctor and A. D. Gilbert (Cambridge University Press, Cambridge, 1994), pp. 181–218.
[22] S. G. Llewellyn Smith and S. M. Tobias, Vortex dynamos, J. Fluid Mech. **498**, 1 (2004).
[23] C. S. Skene and S. M. Tobias, csskene/ABC-dynamo_FTLE: Initial release (2023), https://doi.org/10.5281/zenodo.7565686.
[24] I. Bouya and E. Dormy, Toward an asymptotic behaviour of the ABC dynamo, Europhys. Lett. **110**, 14003 (2015).
[25] See Supplemental Material at http://link.aps.org/supplemental/10.1103/PhysRevFluids.8.083701 for movies of the FTLEs in the kinematic regime over five periods.
[26] G. Haller, Lagrangian coherent structures from approximate velocity data, Phys. Fluids **14**, 1851 (2002).
[27] S. C. Shadden, F. Lekien, and J. E. Marsden, Definition and properties of Lagrangian coherent structures from finite-time Lyapunov exponents in two-dimensional aperiodic flows, Physica D **212**, 271 (2005).
[28] V. Zheligovsky, *Large-Scale Perturbations of Magnetohydrodynamic Regimes Linear and Weakly Nonlinear Stability Theory* (Springer, Heidelberg, 2011).